JAEA-Technology
2007-032

Singular Point Analysis during Rail Deployment into Vacuum Vessel for ITER Blanket Maintenance

Satoshi KAKUDATE and Kiyoshi SHIBANUMA

Tokamak Device Group
Fusion Research and Development Directorate

May 2007

Japan Atomic Energy Agency

日本原子力研究開発機構

JAEA-Technology

本レポートは日本原子力研究開発機構が不定期に発行する成果報告書です。
本レポートの入手並びに著作権利用に関するお問い合わせは、下記あてにお問い合わせ下さい。
なお、本レポートの全文は日本原子力研究開発機構ホームページ（http://www.jaea.go.jp/index.shtml）より発信されています。このほか財団法人原子力弘済会資料センター*では実費による複写頒布を行っております。

〒319-1195　茨城県那珂郡東海村白方白根 2 番地 4
日本原子力研究開発機構　研究技術情報部　研究技術情報課
電話 029-282-6387, Fax 029-282-5920

*〒319-1195　茨城県那珂郡東海村白方白根 2 番地 4　日本原子力研究開発機構内

This report is issued irregularly by Japan Atomic Energy Agency
Inquiries about availability and/or copyright of this report should be addressed to
Intellectual Resources Section, Intellectual Resources Department,
Japan Atomic Energy Agency
2-4 Shirakata Shirane, Tokai-mura, Naka-gun, Ibaraki-ken 319-1195 Japan
Tel +81-29-282-6387, Fax +81-29-282-5920

JAEA-Technology 2007-032

Singular Point Analysis during Rail Deployment into Vacuum Vessel for ITER Blanket Maintenance

Satoshi KAKUDATE and Kiyoshi SHIBANUMA

ITER Project Unit
Fusion Research and Development Directorate
Japan Atomic Energy Agency
Naka-shi, Ibaraki-ken

(Received February 7, 2007)

Remote maintenance of the ITER blanket composed of about 400 modules in the vessel is required by a maintenance robot due to high gamma radiation of ∽500Gy/h in the vessel. A concept of rail-mounted vehicle manipulator system has been developed to apply to the maintenance of the ITER blanket. The most critical issue of the vehicle manipulator system is the feasibility of the deployment of the articulated rail composed of eight rail links into the donut-shaped vessel without any driving mechanism in the rail. To solve this issue, a new driving mechanism and procedure for the rail deployment has been proposed, taking account of a repeated operation of the multi-rail links deployed in the same kinematical manner. The new driving mechanism, which is deferent from those of a usual "articulated arm" equipped with actuator in the every joint for movement, is composed of three mechanisms. To assess the feasibility of the kinematics of the articulated rail for rail deployment, a kinematical model composed of three rail links related to a cycle of the repeated operation for rail deployment was considered. The determinant det J' of the Jacobian matrix J' was solved so as to estimate the existence of a singular point of the transformation during rail deployment. As a result, it is found that there is a singular point due to det J'=0. To avoid the singular point of the rail links, a new location of the second driving mechanism and the related rail deployment procedure are proposed. As a result of the rail deployment test based on the new proposal using a full-scale vehicle manipulator system, the respective rail links have been successfully deployed within 6 h less than the target of 8 h in the same manner of the repeated operation under a synchronized cooperation among the three driving mechanisms. It is therefore concluded that the feasibility of the rail deployment of the articulated rail composed of simple structures without any driving mechanism has been demonstrated.

Keyword: ITER, Blanket Maintenance, Remote Handling. Rail Deployment, Vehicle, Singular Point, Kinematics Analysis, Articulated Rail

JAEA-Technology 2007-032

ITERブランケット保守用軌道の真空容器内への展開時における特異点解析

日本原子力研究開発機構　核融合研究開発部門　ITERプロジェクトユニット
角舘　聡・柴沼　清

（2007年2月7日受理）

真空容器内に設置された約400個からなるブランケットの保守は、真空容器内の放射線レベルが～500Gy/hであるために遠隔保守ロボットにより行われることが要求されている。このため、軌道走行型ビークルマニピュレータ・システムがITERブランケット保守のために採用されている。このビークルマニピュレータ・システムの最も大きな課題は、関節部に駆動源を持たない8リンクから構成された多関節軌道をドーナツ状真空容器内へ展開するための技術的な成立性である。この課題を解決するために、多関節リンクの繰り返し動作を考慮して、新たな軌道展開機構とその手順を提案した。提案された軌道展開機構は一般の関節部に駆動源をもつ多関節アームと異なり3種類の独立したシステムから構成される。軌道展開時における多関節リンクの機構学的な成立性を評価するために、軌道展開時に一連の繰り返し動作に関与する3つの軌道リンクから構成された機構モデルを提案した。このモデルを用いて、多関節軌道の軌道展開時に軌道の姿勢が特定できずに制御が困難となる特異姿勢（特異点）が存在するかどうかを評価した。このため、ヤコビアン行列J'のdet J'を解析的に求めた結果、特異姿勢が存在することが判明した。この特異姿勢を回避するために、三種類の軌道展開システムの第2軌道展開機構について、軌道展開時の新しい動作シナリオを提案した。実規模ビークルマニピュレータ・システムを用いて新提案による軌道展開試験を行った結果、3種類の軌道展開機構の繰り返し動作により、目的の8時間以下の6時間で多関節軌道が全て展開できることが実証された。これにより、軌道に駆動源を持たない多関節軌道の軌道展開に関する成立性が確認された。

那珂核融合研究所（駐在）：〒311－0193　茨城県那珂市向山801－1

Contents

目次

1. Introduction

ITER (International Thermonuclear Experimental Reactor) is planned to demonstrate the scientific and technological feasibility of fusion energy for peaceful purposes under an international collaboration of Japan, the European Atomic Energy Community and the Russian Federation [1]. Components in the ITER vessel will be activated because of 14 MeV neutrons arising from the fusion reactions. Maintenance of the components such as blanket inside the vessel has to be carried out under an intense gamma radiation of ∽500Gy/h. All interventions in the vessel must therefore be performed remotely by a maintenance robot. In particular, the maintenance of the blanket is identified as the most important activity in the ITER remote maintenance. For local maintenance, the blanket is divided into about 400 modules and individually replaced. The typical blanket module is a box shaped configuration with a weight of 4 t and a dimension of 2 x 1.5 x 0.5 m. It is a requirement to the maintenance robot that the 4-t blanket module is installed under a clearance of 0.25 mm between the groove of the module and the key of the vessel [1), 2)]. A concept of rail-mounted vehicle manipulator system has been proposed to meet the requirement [3), 4)]. Figure 1 shows a basic layout of the vehicle manipulator system applied to the blanket module maintenance in the donut-shaped ITER vessel [4)]. The vehicle manipulator system composed of the articulated rail, vehicle manipulator and rail deployment base is transported by transfer casks, which are docked at two maintenance ports located at the 0 and 180 degree ports. The rail has to be deployed from the transfer cask and forms a toroidal ring in the vessel so as to access all blanket modules inside the vessel. After deployment, the rail is supported at the four orthogonal maintenance ports[1)]. The system has the following potentials[3)]: (1) stable handling of the heavy blanket modules with high positional accuracy due to high stiffness of the toroidal rail as a base structure, (2) simple articulated rail structure without any sensitive elements such as actuators and sensors for rail deployment and (3) parallel operations of several vehicle manipulators on the common rail to minimize the maintenance time.

The most critical issue of the system so as to apply to the ITER blanket maintenance is the feasibility of the deployment of the articulated rail composed of simple structures into the vessel without any driving mechanism in the rail.

This paper describes a rail deployment scenario and the related kinematical analysis for rail deployment, together with the result of the proof of principle test on the rail deployment using a full-scale vehicle manipulator system.

2. Rail deployment procedure and driving mechanisms

The vehicle system is transported to the maintenance ports via a transfer cask. Figure 2 shows an initial configuration of the articulated rail composed of laterally flexible eight rail links connected by hinges at the respective joints before rail deployment. Figure 3 illustrates a candidate of the rail deployment procedure of a representative rail link. The rail deployment can be carried out by a repeated operation, i.e., the respective rail links can be deployed into the vessel by the repeated operation in the same sequential manner. Taking notice of the repeated operation for rail deployment, the number of driving mechanisms can be minimized. According to the deployment procedure shown in Fig. 3, the driving mechanisms are required at least for toroidal movement in the vessel and for radial movement in the maintenance port without uncontrolled kink of the laterally flexible articulated rail. For toroidal movement, a traveling mechanism of the vehicle, which is used for movement along the toroidal rail deployed in the vessel, is the most useful candidate of the driving mechanism for toroidai movement of the rail in the vessel. That is, the rail can be fed into the vessel by the operation of the vehicle traveling mechanism under the conditions that the rail is free without any constraint and the vehicle is fixed somewhere. For radial movement, two driving mechanisms are required to prevent the articulated rail from the uncontrolled kink in the port (in particular during storage operation). Consequently, at least three driving mechanisms are required to deploy the articulated rain in the vessel.

(a) Rail deployment scenario (1)

Three driving mechanisms d_1, d_2 and d_3 are allocated, respectively, as shown in Fig. 3, and can deploy the respective rail links under a cooperation of position-based control among them. The relation among the three driving mechanisms d_1, d_2 and d_3 is shown in Fig. 4. This is called as a rail deployment scenario (1). The repeated operation for rail deployment is dominated by the first and second driving mechanisms d_1 and d_2 because the operation of the third driving mechanism d_3 is just followed according to the movement of the second driving mechanism d_2. Therefore, the rail deployment is simply carried out by the two rail links driven by the driving mechanisms d_1 and d_2 in the deployment scenario (1). However, since the second driving mechanism d_2 in the Stage (4) and (5) is positioned inside the vessel apart from the maintenance port as shown in Figs. 3 and 4, the high power driving mechanism d_2 for rail deployment can not be located in the vessel through the restricted maintenance port.

(b) Rail deployment scenario (2)

To solve the problem on the space restriction to install the second driving mechanism d_2 for rail deployment, the location of the driving mechanism d_2 is changed to that of d_2', which is shifted backward by one rail link as shown in Fig. 3. This new scenario is called as a rail deployment scenario (2). In this case, the movable space of the driving mechanism d_2' can be kept within the maintenance port as shown in Figs. 3 and 5. However, the kinematics in the scenario (2) will be more complicated than that in the scenario (1), because the number of the rail links related to the repeated operation driven by the driving mechanisms d_1 and d_2 is increased to three in the scenario (2) from two in the scenario (1), i.e., one degree of freedom of the rail links related to the repeated operation is increased in the scenario (2). The following analysis is therefore performed so as to assess the feasibility of the kinematics of the articulated rail for rail deployment based on the scenario (2).

3. Singular point analysis for rail deployment

Figure 6 shows a kinematical analysis model for rail deployment. The model is composed of three rail links l_{i-1}, l_i and l_{i+1} due to repeated operation for rail deployment. The rail link l_{i-1}, which is deployed in the toroidal direction, is simplified as an "imaginary rail link l'_{i-1}" indicating the position vector $\mathbf{P}_i$ of the rail link l_{i-1}. Using the imaginary rail link l'_{i-1}, the three rail linked structure becomes an equivalent articulated structure composed of three links of a usual manipulator. Therefore, the position vector $\mathbf{P}_{i+2}$ of the rail link l_{i+1} is given by the following equation using the respective rail link vectors $\mathbf{l'}_{i-1}$, $\mathbf{l}_i$ and $\mathbf{l}_{i+1}$ [5).].

$$\mathbf{P}_{i+2} = {}^0R_0\mathbf{l'}_{i-1} + {}^0R_i\mathbf{l}_i + {}^0R_{i+1}\mathbf{l}_{i+1}$$

$$= \begin{bmatrix} P_{x,i+2} \\ P_{y,i+2} \end{bmatrix} = \begin{bmatrix} l'_{i-1}\cos(\theta_{i-1}) + l_i\cos(\theta_{i-1}+\theta_i) + l_{i+1}\cos(\theta_{i-1}+\theta_i+\theta_{i+1}) \\ l'_{i-1}\sin(\theta_{i-1}) + l_i\sin(\theta_{i-1}+\theta_i) + l_{i+1}\sin(\theta_{i-1}+\theta_i+\theta_{i+1}) \end{bmatrix} \quad (1)$$

where

$\mathbf{l}_i$: i-th rail link vector, $l_i = |\mathbf{l}_i|$: length of i-th rail link

$\mathbf{l'}_{i-1}$: imaginary rail link, $l'_{i-1} = |\mathbf{l'}_{i-1}|$: length of imaginary rail link

θ_i : joint angle between two rail links $\mathbf{l}_{i-1}$ and $\mathbf{l}_i$

${}^jR_i$: coordinate rotation matrix of i-th rail joint around the z-axis from the reference point of the j-th rail joint. Therefore, the respective coordinate rotation matrixes around the z-axis from the reference point of the origin O are given as follows.

$${}^0R_0 = E^{\mathbf{k}\theta_{i-1}}, \quad {}^0R_i = E^{\mathbf{k}(\theta_{i-1}+\theta_i)}, \quad {}^0R_{i+1} = E^{\mathbf{k}(\theta_{i-1}+\theta_i+\theta_{i+1})}$$

$$E^{\mathbf{k}\theta} = \begin{pmatrix} \cos\theta & -\sin\theta & 0 \\ \sin\theta & \cos\theta & 0 \\ 0 & 0 & 1 \end{pmatrix}$$

The position vector $\mathbf{P}_{i+2}$ in the equation (1) cannot be determined since the kinematical model in Fig. 6 contains one redundant degree of freedom. Therefore, to determine the $\mathbf{P}_{i+2}$, the rail link vector $\mathbf{l}_{i+1}$ is positioned in parallel with the x-axis with an offset of Δ, based on the basic rail deployment scenario shown in Fig. 3. The position vectors $\mathbf{P}_{i+1}$ and $\mathbf{P}_{i+2}$, and the joint angles θ_i and θ_{i+1} are thus given as follows, respectively.

$$\mathbf{P}_{i+1} = \begin{bmatrix} P_{x,i+1} \\ P_{y,i+1} \end{bmatrix} = \begin{bmatrix} l'_{i-1}\cos(\theta_{i-1}) \pm \sqrt{l_i^2 - (\Delta - l'_{i-1}\sin(\theta_{i-1}))^2} \\ \Delta \end{bmatrix} \quad (2)$$

$$\theta_i = \tan^{-1}\left[\frac{-\sin\theta_{i-1}(P_{x,i+1} - l'_{i-1}\cos(\theta_{i-1})) + \cos\theta_{i-1}(P_{y,i+1} - l'_{i-1}\sin(\theta_{i-1}))}{\cos\theta_{i-1}(P_{x,i+1} - l_{i-1}\cos(\theta_{i-1})) + \sin\theta_{i-1}(P_{y,i+1} - l'_{i-1}\sin(\theta_{i-1}))}\right] \quad (3)$$

$$\mathbf{P}_{i+2} = \mathbf{P}_{i+1} + \mathbf{l}_{i+2} = \begin{bmatrix} P_{x,i+2} \\ P_{y,i+2} \end{bmatrix} = \begin{bmatrix} P_{x,i+1} + l_{i+2} \\ \Delta \end{bmatrix} \tag{4}$$

$$\theta_{i+1} = \tan^{-1}\left[\frac{P_{y,i+2} - \left(l'_{i-1}\sin(\theta_{i-1}) + l_i \sin(\theta_{i-1} + \theta_i)\right)}{P_{x,i+2} - \left(l'_{i-1}\cos(\theta_{i-1}) + l_i \cos(\theta_{i-1} + \theta_i)\right)}\right] - \left(\theta_i + \theta_{i-1}\right) \tag{5}$$

The velocity vector $\dot{\mathbf{P}}_{i+2}$ of the position vector $\mathbf{P}_{i+2}$ is defined by the following equation.

$$\dot{\mathbf{P}}_{i+2} = J\dot{\theta} \tag{6}$$

where

$$\dot{\mathbf{P}} = (\dot{P}_{x,i+2}, \dot{P}_{y,i+2}, \dot{\Phi}_{z,i+2}) \quad , \quad \dot{\theta} = (\dot{\theta}_{i-1}, \dot{\theta}_i, \dot{\theta}_{i+1})$$

J : Jacobian matrix

$$J = \begin{bmatrix} a_{11} & a_{12} & a_{13} \\ a_{21} & a_{22} & a_{23} \\ a_{31} & a_{32} & a_{33} \end{bmatrix}$$

$$a_{11} = \frac{\partial P_{x,i+2}}{\partial \theta_{i-1}} = -\left[l'_{i-1}\sin(\theta_{i-1}) + l_i \sin(\theta_{i-1} + \theta_i) + l_{i+1}\sin(\theta_{i-1} + \theta_i + \theta_{i+1})\right]$$

$$a_{12} = \frac{\partial P_{x,i+2}}{\partial \theta_i} = -\left[l_i \sin(\theta_{i-1} + \theta_i) + l_{i+1}\sin(\theta_{i-1} + \theta_i + \theta_{i+1})\right]$$

$$a_{13} = \frac{\partial P_{x,i+2}}{\partial \theta_{i+1}} = -\left[l_{i+1}\sin(\theta_{i-1} + \theta_i + \theta_{i+1})\right]$$

$$a_{21} = \frac{\partial P_{y,i+2}}{\partial \theta_{i-1}} = l'_{i-1}\cos(\theta_{i-1}) + l_i \cos(\theta_{i-1} + \theta_i) + l_{i+1}\cos(\theta_{i-1} + \theta_i + \theta_{i+1})$$

$$a_{22} = \frac{\partial P_{y,i+2}}{\partial \theta_i} = l_i \cos(\theta_{i-1} + \theta_i) + l_{i+1}\cos(\theta_{i-1} + \theta_i + \theta_{i+1})$$

$$a_{23} = \frac{\partial P_{y,i+2}}{\partial \theta_{i+1}} = l_{i+1}\cos(\theta_{i-1} + \theta_i + \theta_{i+1})$$

$$a_{31} = \frac{\partial \Phi_{z,i+2}}{\partial \theta_{i-1}} = 1, a_{32} = \frac{\partial \Phi_{z,i+2}}{\partial \theta_i} = 1, a_{33} = \frac{\partial \Phi_{z,i+2}}{\partial \theta_{i+1}} = 1$$

The imaginary rail link vector $\mathbf{l'}_{i-1}$, which defines only the position and velocity of the i-th rail joint, is not a real link vector. Therefore, the Jacobian matrix J' on the rail link vectors $\mathbf{l}_i$ and $\mathbf{l}_{i+1}$, which are directly related to the motion for rail deployment, is given as follows from the equation (6).

$$J' = \begin{bmatrix} a_{12} & a_{13} \\ a_{22} & a_{23} \end{bmatrix} \tag{7}$$

The determinant of the Jacobian matrix J' is given by

$$\det J' = a_{12}a_{23} - a_{13}a_{22} \tag{8}$$

The determinant $\det J'$ of the equation (8) is solved using the equations (2) to (5). The calculation was carried out under the following conditions, i.e., the offset of the rail link vector $\mathbf{l}_{i+1}$ $\Delta = P_{y,i+2}$= 0.213 m and the lengths of the rail links l_{i-1}= 8.26 m, $l_i = l_{i+1}$= 3.01 m. The calculation result of $\det J'$ is shown in Fig. 7, as a parameter of the position of $P_{x,i+2}$. Due to the determinant $\det J'$ =0 in Fig. 7, it is found that there is a singular point of the transformation during rail deployment. The configuration of the rail links during rail deployment at the $\det J'$ =0 is given by the three joint angles θ_{i-1}= - 1.48, θ_i= 1.48 and θ_{i+1}= 0, and the position of the rail joint $P_{x,i+2}$= 14.3 m. Considering the rail deployment scenario (2) proposed in the section 2, it is found that the configuration of the rail links during rail deployment contains the singular point of the transformation around the Stage (2) between Stages (1) and (3) in Figs. 3 and 5 corresponding to $\det J'$ =0 in Fig. 7. To avoid the singular point, it is the most effective to decrease the degrees of freedom of the rail link structure related to the repeated operation around the Stage (2), e.g., the number of the related rail links is reduced to two from three. Therefore, the location of the second driving mechanism d_2' has to be changed so as to decrease the degrees of freedom of the rail link structure related to the repeated operation around the Stage (2) in Figs. 3 and 5. Figures 8 and 9 show a new proposal on the location and the traveling scenario of the second driving mechanism d_2'' for rail deployment so as to avoid the singular point, respectively. The proposal is a combination of the two rail deployment scenarios (1) and (2) described in the section 2. The location of the driving mechanism d_2'' is the same as that of the scenario (1) from the Stage (1) to (3). The location of d_2'' is however changed at the Stage (4), i.e., from that of the scenario (1) to the scenario (2). According to this new scenario, not only the singular point of the transformation during rail deployment can be avoided, but also the location of d_2'' can be kept in the maintenance port as shown in Fig. 9.

4. Rail deployment test

The proof of principle test for rail deployment of the articulated rail was carried out using a full-scale vehicle manipulator system, which is composed of a vehicle with manipulator, an articulated rail connected by eight rail links, two rail deployment bases, a vehicle fixture arm and a simulated port. The second and third driving mechanisms are installed in the rail deployment bases, respectively. The vehicle is fixed by the vehicle fixture arm during rail deployment. Figure 10 shows the vehicle manipulator system under rail deployment test. As a result of the test, the respective rail links have been successfully deployed up to 180 degrees in the toroidal direction in the vessel within 6 h less than the target of 8 h in the same manner of the repeated operations by the synchronized cooperation based on the teaching playback control among the three driving mechanisms without any diving mechanisms in the rail structure. The number of the teaching playback data is 92 for rail deployment. Figure 11 shows a typical test result on the rail deployment of the six rail links by the repeated operations after the first two rail links were inserted and deployed together with the vehicle in the toroidal direction by the vehicle fixture arm. The circles and solid lines in Fig. 11 show the teaching playback data and the test results of the traveling traces of the second and third driving mechanisms during rail deployment, respectively. The results of the last two rail links are deferent from those of the other rail links. This is because the synchronized cooperation among the three driving mechanisms is not required due to the reduction of the degrees of the freedom for rail deployment in the case of the last two rail links. In addition, the storage of the articulated rail has also been demonstrated in the same manner according to the reverse procedures of the rail deployment. It is therefore concluded that the feasibility of the rail deployment of the articulated rail composed of simple structures without any driving mechanism has been demonstrated without any trouble caused by the singular point of the transformation during rail deployment.

5. Conclusion

The most critical issue of the vehicle manipulator system for blanket maintenance is the feasibility of the deployment of the articulated rail composed of eight rail links into the donut-shaped vessel without any driving mechanism in the rail. To solve this issue, a new driving mechanism and procedure for the rail deployment has been proposed, taking account of the repeated operation of the multi-rail links deployed in the same kinematical manner. The new driving mechanism, which is deferent from those of a usual “articulated arm” equipped with actuator in the every joint for movement, is composed of three mechanisms. To assess the feasibility of the kinematics of the articulated rail for rail deployment, a kinematical model composed of three links related to a cycle of the repeated operation for rail deployment was considered. The determinant $\det J'$ of the Jacobian matrix J' was solved so as to estimate the existence of a singular point of the transformation during rail deployment. As a result, it is found that there is a singular point for rail deployment due to $\det J' = 0$. To avoid the singular point of the rail links, a new location of the second driving mechanism and the related rail deployment procedure were proposed. As a result of the rail deployment test based on the new proposal using the full-scale vehicle manipulator system, the respective rail links have been successfully deployed within 6 h less than the target of 8 h in the same manner of the repeated operation under the synchronized cooperation among the three driving mechanisms. The storage of the articulated rail has also been demonstrated in the same manner according to the reverse procedures of the rail deployment. It is therefore concluded that the feasibility of the rail deployment of the articulated rail composed of simple structures without any driving mechanism has been demonstrated.

Acknowledgments

The author would like to acknowledge Drs. T. Tsunematsu and R. Yoshino of Japan Atomic Energy Agency for their continuous suggestions and encouragement.

References

1) “ITER Technical Basis”, ITER EDA Documentation Series No. 24, IAEA, Vienna, 2002.

2) M. Mori, et al., “The Summary Report on Engineering Design Activities in the International Thermonuclear Experimental Rector (ITER) Project”, J. the Atomic Energy Society of Japan, 44, 16-89 (2002).

3) K. Shibanuma, et al., “Development of In-vessel Remote Maintenance System for Fusion Experimental Reactor (FER)”, Proc. of ’91 Int. Sympo. on Advanced Robot Technology (’91 ISART), 127-133 (1991).

4) K. Shibanuma, et al., “Blanket Remote Handling Systems”, Fusion Eng. Des., 55, 249-257 (2001).

5) S. Hirose, “Robotics-Vector Analysis of Mechanical System-”, Shokabo, Tokyo (1987).

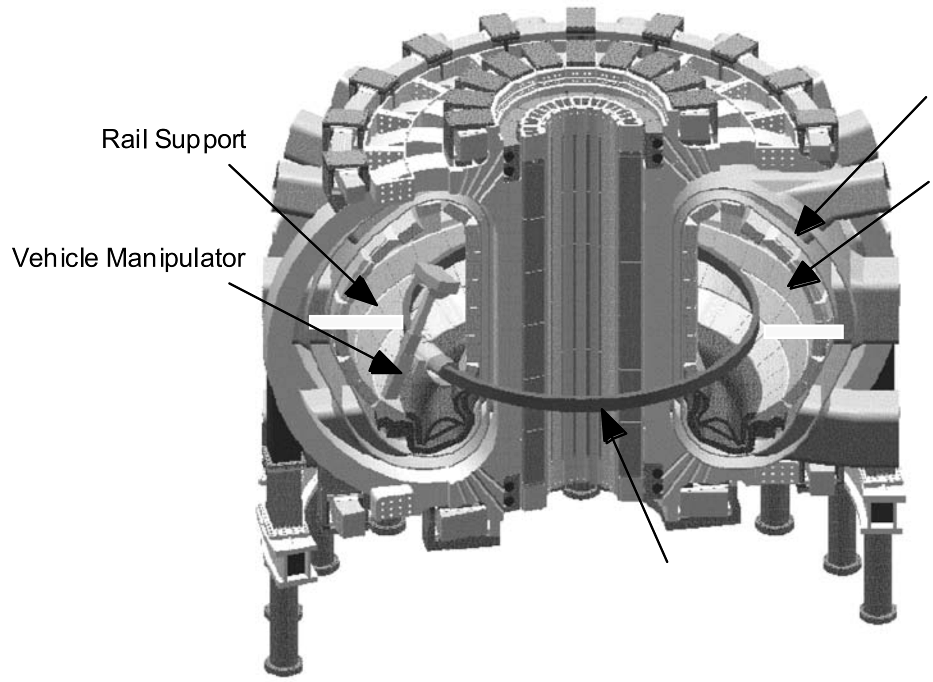

Fig. 1 Vehicle manipulator system for blanket maintenance

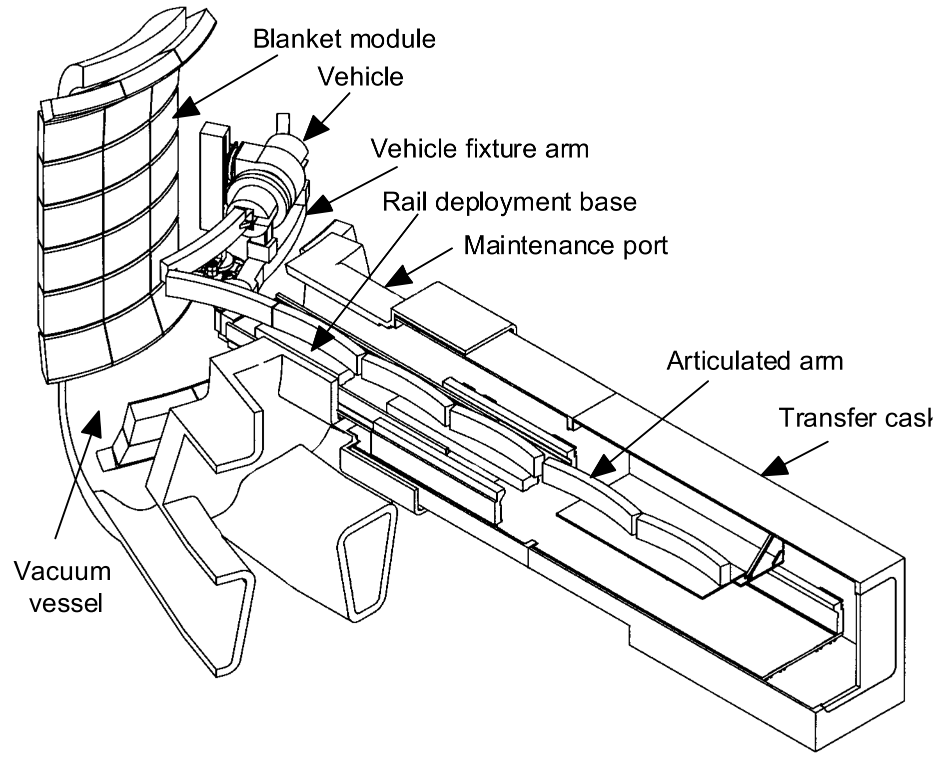

Fig. 2 Initial configuration of the articulated rail of the vehicle manipulator system for rail deployment in the maintenance port and transfer cask

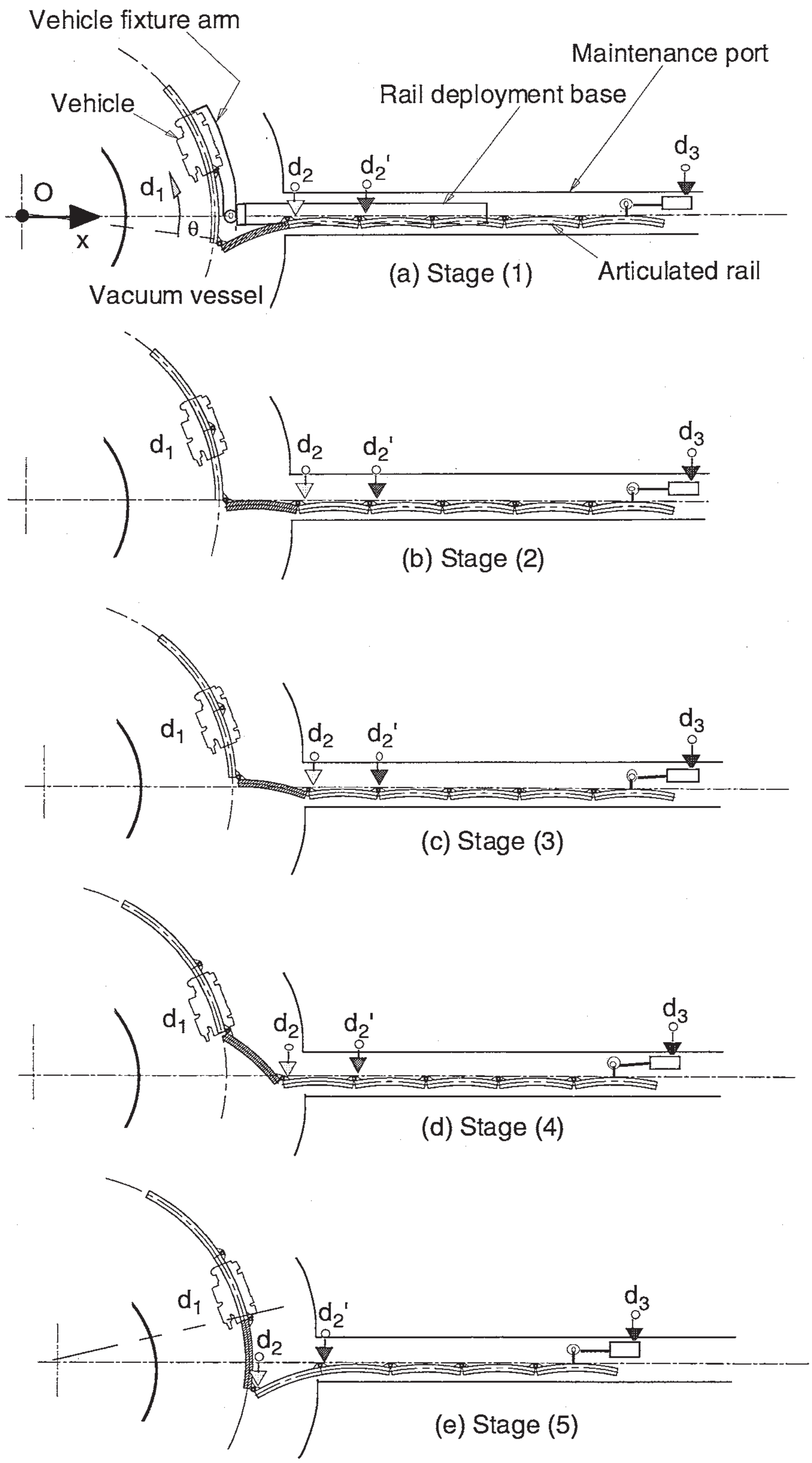

Fig. 3 Rail deployment procedure of a representative rail link using three driving mechanisms d_1, d_2 (or d_2') and d_3. The second driving mechanisms d_2 and d_2' are used for the rail deployment scenario (1) and (2), respectively.

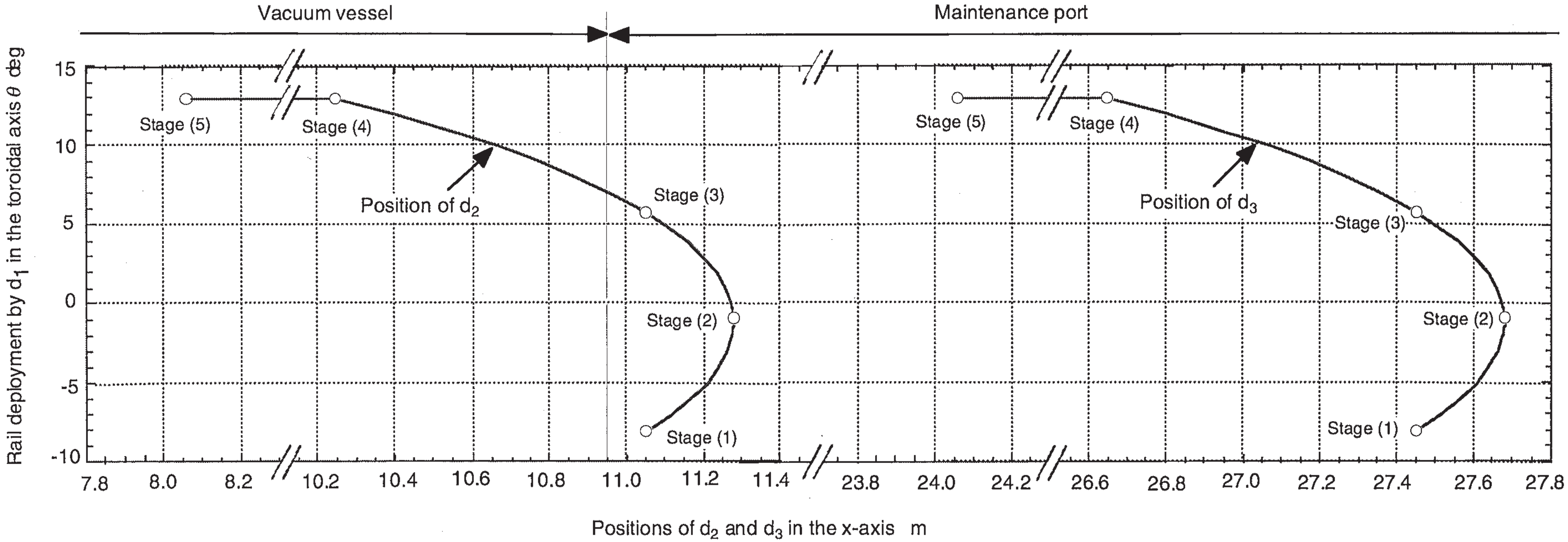

Fig. 4 Positional relationship among three driving mechanisms d_1, d_2 and d_3 under one cycle sequence of the repeated operations (rail deployment scenario (1))

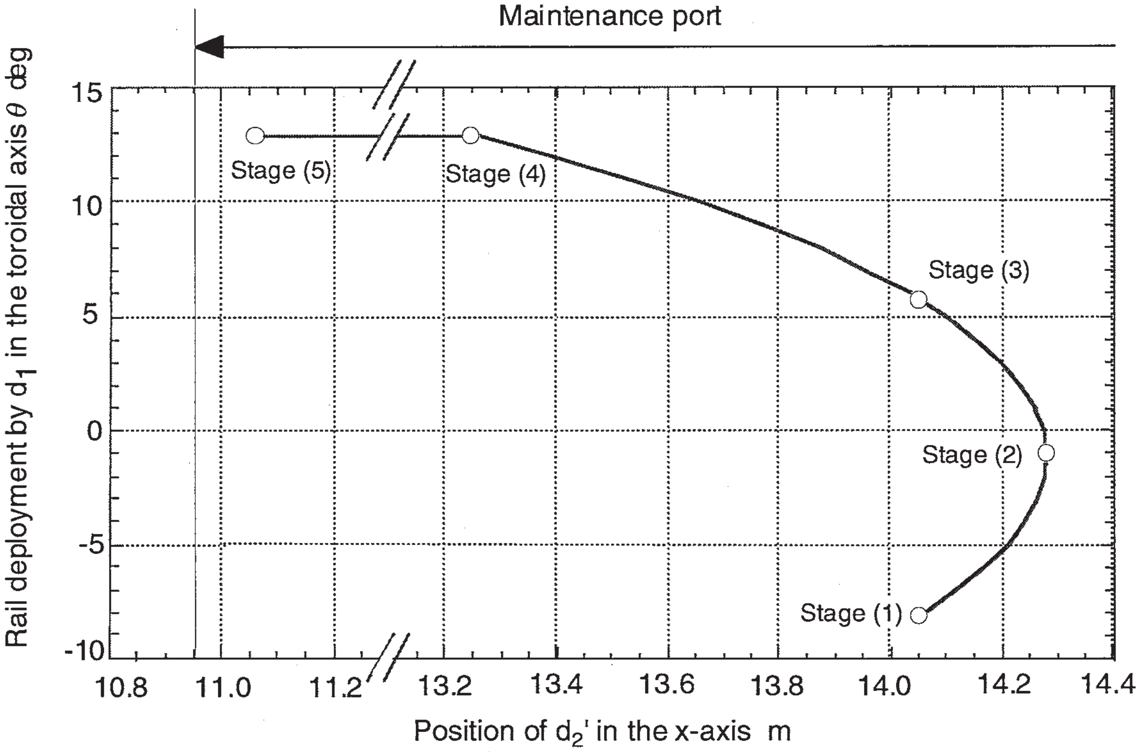

Fig. 5 Positional relationship between two driving mechanisms d_1 and d_2' under one cycle sequence of the repeated operations (rail deployment scenario (2))

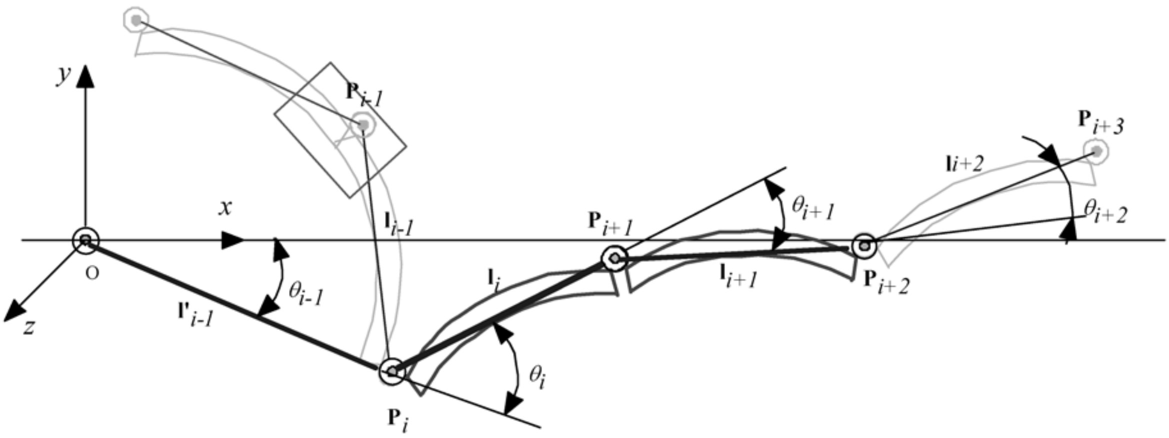

Fig. 6 Kinematical analysis model for rail deployment

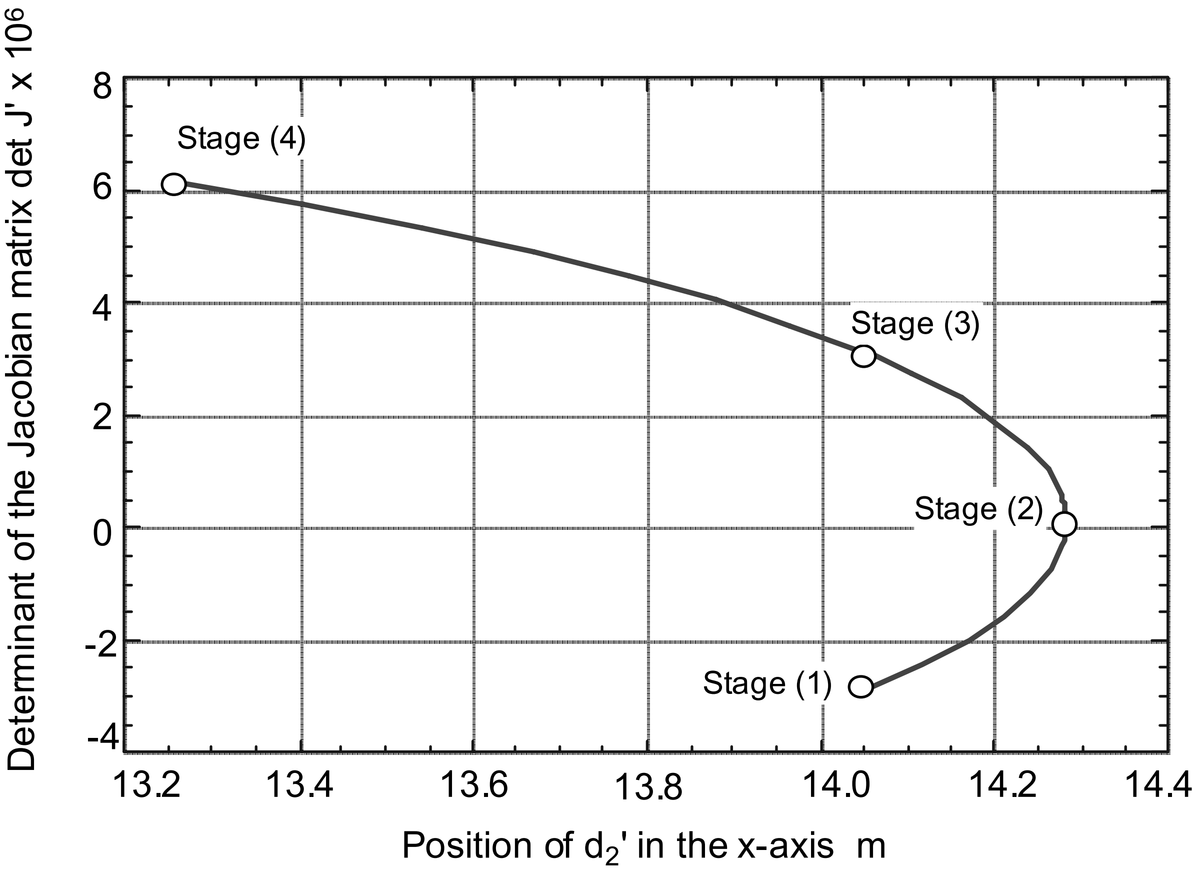

Fig. 7 Calculation result of the determinant of the Jacobian matrix det J' based on the rail deployment scenario (2)

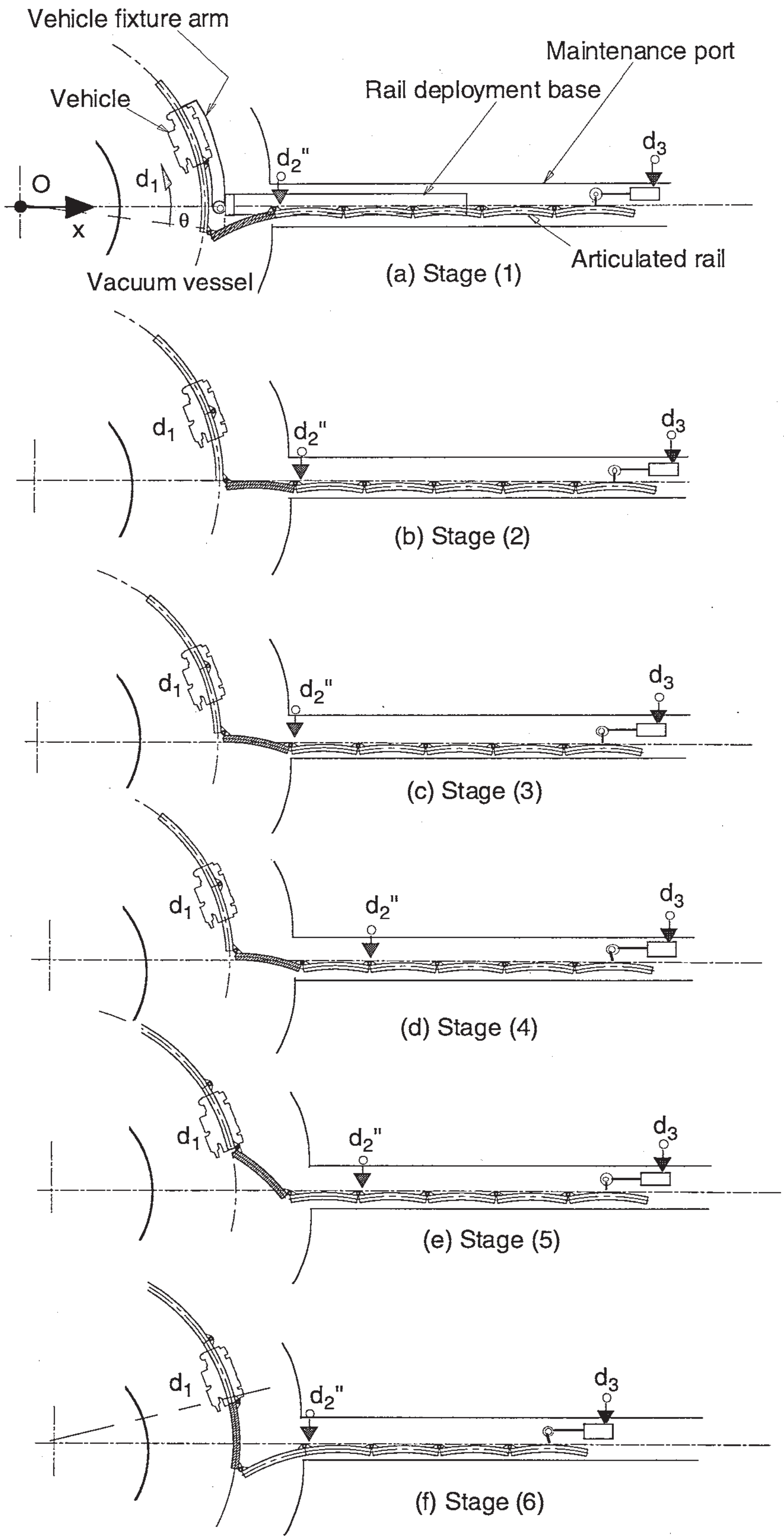

Fig. 8 New proposal of the location of the driving mechanism d_2'' and the rail deployment procedure

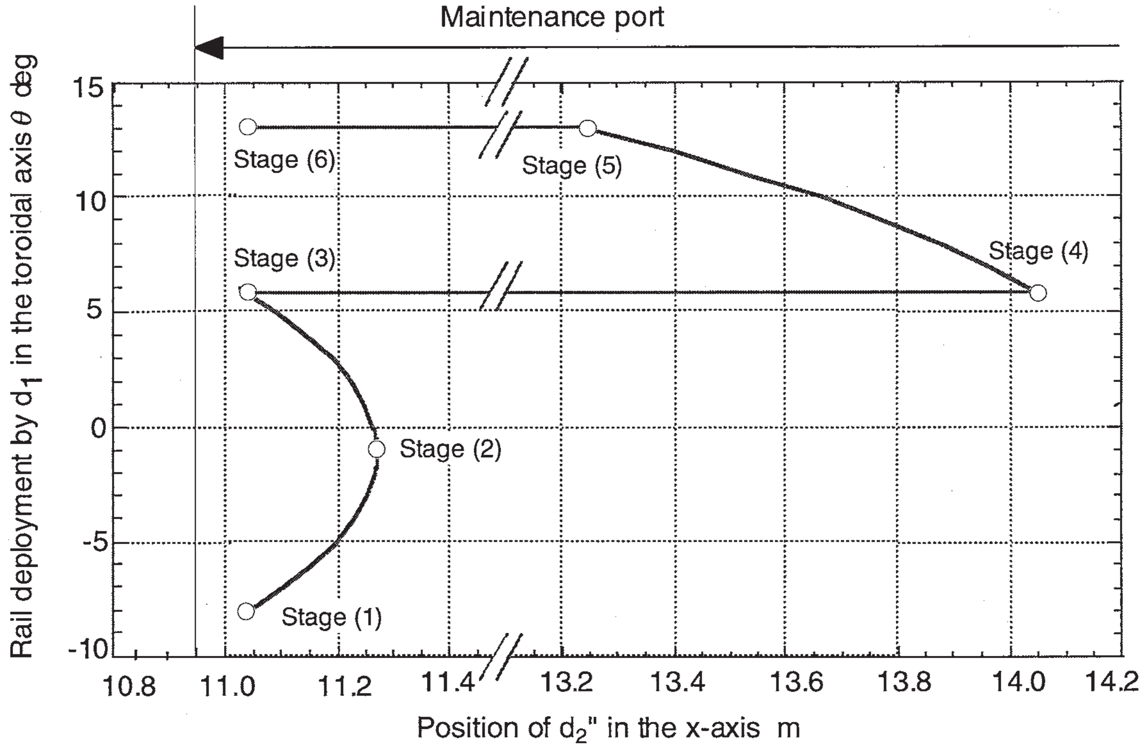

Fig. 9 New positional relationship between two driving mechanisms d_1 and d_2'' under one cycle sequence of the repeated operations

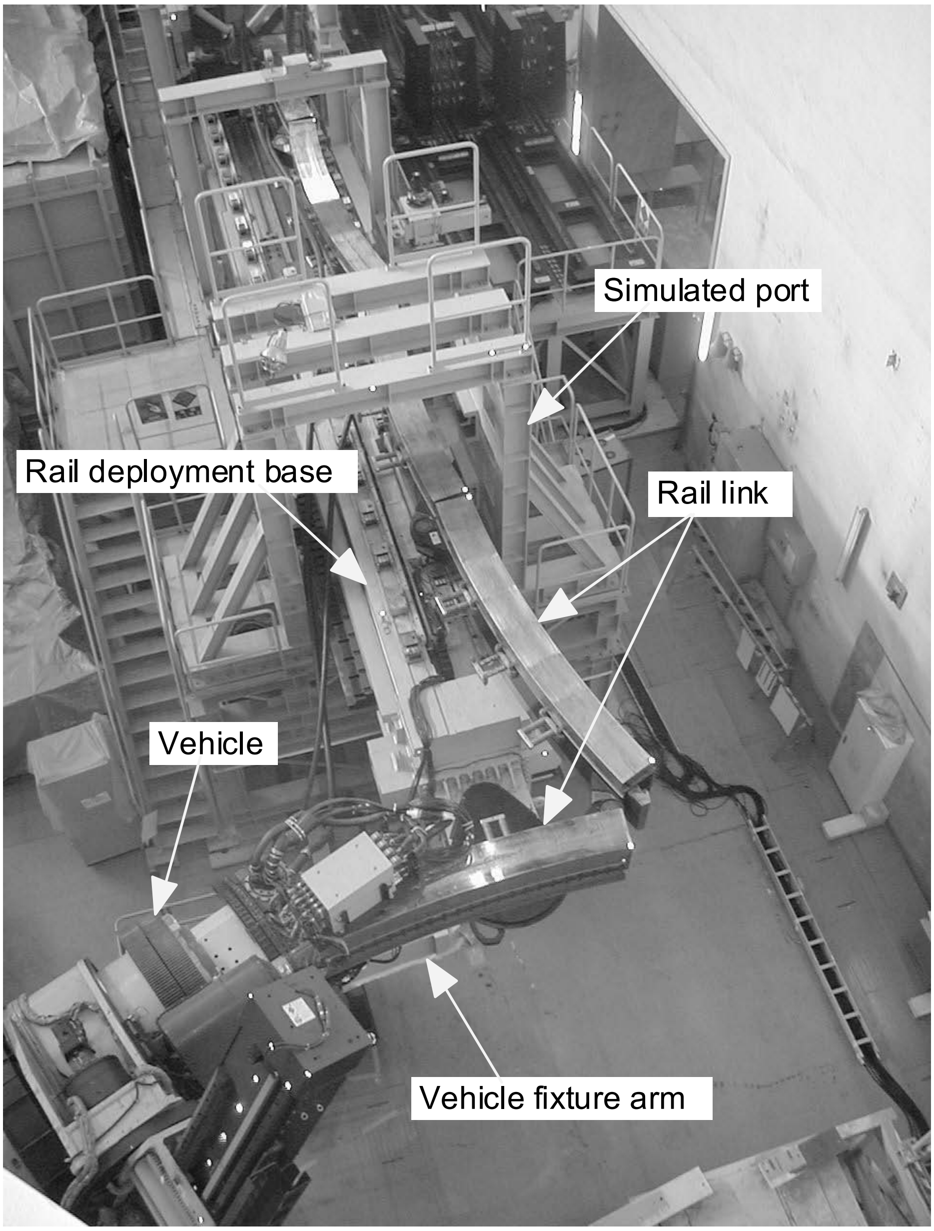

Fig. 10 Full-scale vehicle manipulator system under rail deployment test

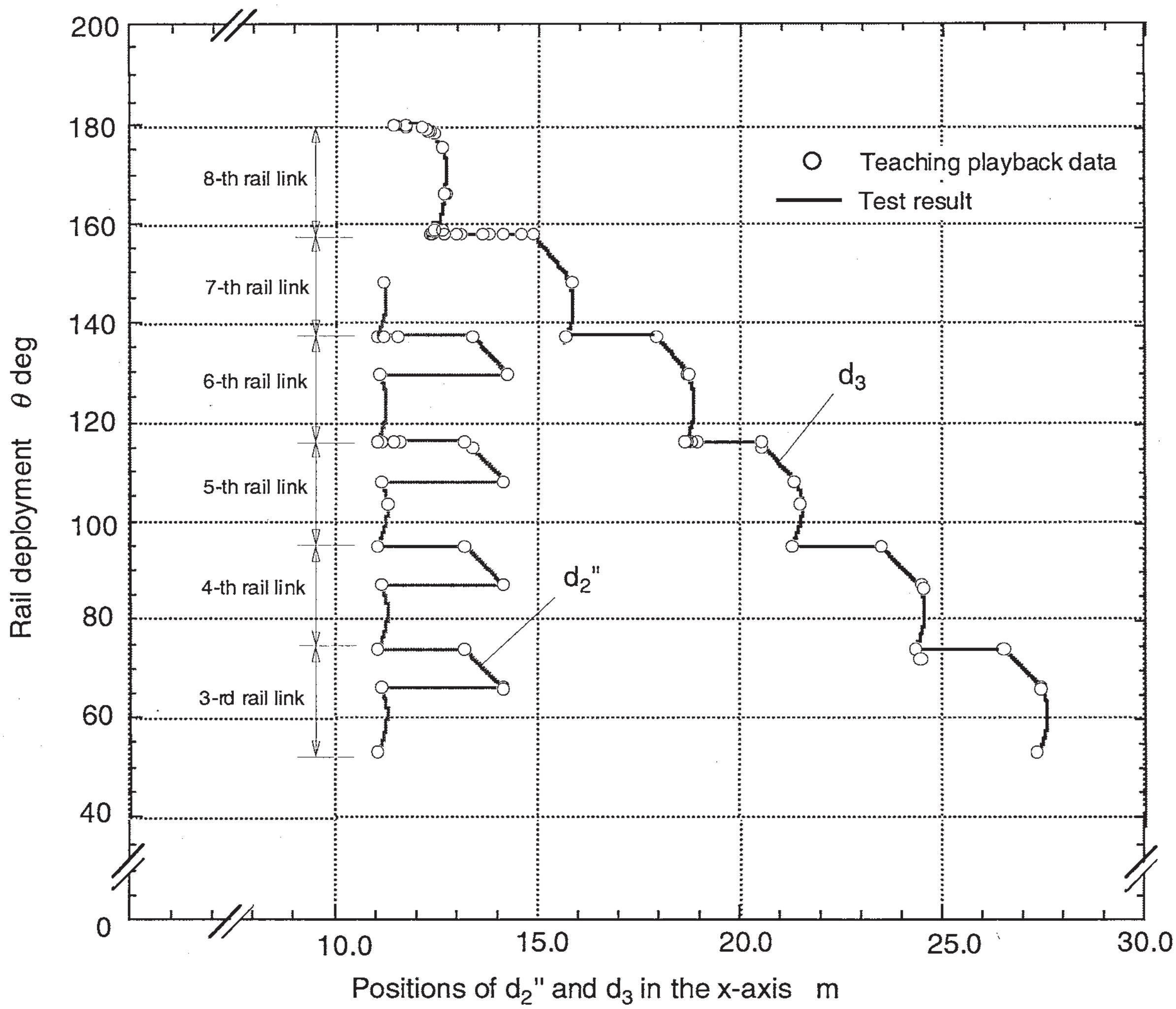

Fig. 11 Typical test result on the rail deployment up to 180 degrees by the repeated operations

国際単位系（SI）

表１．SI 基本単位

基本量	SI 基本単位	
	名称	記号
長さ	メートル	m
質量	キログラム	kg
時間	秒	s
電流	アンペア	A
熱力学温度	ケルビン	K
物質量	モル	mol
光度	カンデラ	cd

表２．基本単位を用いて表されるSI組立単位の例

組立量	SI 基本単位	
	名称	記号
面積	平方メートル	m^2
体積	立法メートル	m^3
速さ，速度	メートル毎秒	m/s
加速度	メートル毎秒毎秒	m/s^2
波数	毎メートル	m-1
密度（質量密度）	キログラム毎立法メートル	kg/m^3
質量体積（比体積）	立法メートル毎キログラム	m^3/kg
電流密度	アンペア毎平方メートル	A/m^2
磁界の強さ	アンペア毎メートル	A/m
（物質量の）濃度	モル毎立方メートル	mol/m^3
輝度	カンデラ毎平方メートル	cd/m^2
屈折率	（数の）1	1

表５．SI 接頭語

乗数	接頭語	記号	乗数	接頭語	記号
10^{24}	ヨタ	Y	10^{-1}	デシ	d
10^{21}	ゼタ	Z	10^{-2}	センチ	c
10^{18}	エクサ	E	10^{-3}	ミリ	m
10^{15}	ペタ	P	10^{-6}	マイクロ	μ
10^{12}	テラ	T	10^{-9}	ナノ	n
10^{9}	ギガ	G	10^{-12}	ピコ	p
10^{6}	メガ	M	10^{-15}	フェムト	f
10^{3}	キロ	k	10^{-18}	アト	a
10^{2}	ヘクト	h	10^{-21}	ゼプト	z
10^{1}	デカ	da	10^{-24}	ヨクト	y

表３．固有の名称とその独自の記号で表されるSI組立単位

組立量	SI 組立単位			
	名称	記号	他のSI単位による表し方	SI基本単位による表し方
平面角	ラジアン(a)	rad		$m \cdot m^{-1}=1$(b)
立体角	ステラジアン(a)	sr(c)		$m^2 \cdot m^{-2}=1$(b)
周波数	ヘルツ	Hz		s^{-1}
力	ニュートン	N		$m \cdot kg \cdot s^{-2}$
圧力，応力	パスカル	Pa	N/m^2	$m^{-1} \cdot kg \cdot s^{-2}$
エネルギー，仕事，熱量	ジュール	J	N・m	$m^2 \cdot kg \cdot s^{-2}$
工率，放射束	ワット	W	J/s	$m^2 \cdot kg \cdot s^{-3}$
電荷，電気量	クーロン	C		s・A
電位差（電圧），起電力	ボルト	V	W/A	$m^2 \cdot kg \cdot s^{-3} \cdot A^{-1}$
静電容量	ファラド	F	C/V	$m^{-2} \cdot kg^{-1} \cdot s^4 \cdot A^2$
電気抵抗	オーム	Ω	V/A	$m^2 \cdot kg \cdot s^{-3} \cdot A^{-2}$
コンダクタンス	ジーメンス	S	A/V	$m^{-2} \cdot kg^{-1} \cdot s^3 \cdot A^2$
磁束	ウエーバ	Wb	V・s	$m^2 \cdot kg \cdot s^{-2} \cdot A^{-1}$
磁束密度	テスラ	T	Wb/m^2	$kg \cdot s^{-2} \cdot A^{-1}$
インダクタンス	ヘンリー	H	Wb/A	$m^2 \cdot kg \cdot s^{-2} \cdot A^{-2}$
セルシウス温度	セルシウス度(d)	℃		K
光束	ルーメン	lm	cd・sr(c)	$m^2 \cdot m^{-2} \cdot cd=cd$
照度	ルクス	lx	lm/m^2	$m^2 \cdot m^{-4} \cdot cd=m^{-2} \cdot cd$
（放射性核種の）放射能	ベクレル	Bq		s^{-1}
吸収線量，質量エネルギー分与，カーマ	グレイ	Gy	J/kg	$m^2 \cdot s^{-2}$
線量当量，周辺線量当量，方向性線量当量，個人線量当量，組織線量当	シーベルト	Sv	J/kg	$m^2 \cdot s^{-2}$

(a)ラジアン及びステラジアンの使用は、同じ次元であっても異なった性質をもった量を区別するときの組立単位の表し方として利点がある。組立単位を形作るときのいくつかの用例は表４に示されている。
(b)実際には、使用する時には記号rad及びsrが用いられるが、習慣として組立単位としての記号"１"は明示されない。
(c)測光学では、ステラジアンの名称と記号srを単位の表し方の中にそのまま維持している。
(d)この単位は、例としてミリセルシウス度m℃のようにSI接頭語を伴って用いても良い。

表４．単位の中に固有の名称とその独自の記号を含むSI組立単位の例

組立量	SI 組立単位		
	名称	記号	SI 基本単位による表し方
粘度	パスカル秒	Pa・s	$m^{-1} \cdot kg \cdot s^{-1}$
力のモーメント	ニュートンメートル	N・m	$m^2 \cdot kg \cdot s^{-2}$
表面張力	ニュートン毎メートル	N/m	$kg \cdot s^{-2}$
角速度	ラジアン毎秒	rad/s	$m \cdot m^{-1} \cdot s^{-1}=s^{-1}$
角加速度	ラジアン毎平方秒	rad/s^2	$m \cdot m^{-1} \cdot s^{-2}=s^{-2}$
熱流密度，放射照度	ワット毎平方メートル	W/m^2	$kg \cdot s^{-3}$
熱容量，エントロピー	ジュール毎ケルビン	J/K	$m^2 \cdot kg \cdot s^{-2} \cdot K^{-1}$
質量熱容量（比熱容量），質量エントロピー	ジュール毎キログラム毎ケルビン	J/(kg・K)	$m^2 \cdot s^{-2} \cdot K^{-1}$
質量エネルギー（比エネルギー）	ジュール毎キログラム	J/kg	$m^2 \cdot s^{-2} \cdot K^{-1}$
熱伝導率	ワット毎メートル毎ケルビン	W/(m・K)	$m \cdot kg \cdot s^{-3} \cdot K^{-1}$
体積エネルギー	ジュール毎立方メートル	J/m^3	$m^{-1} \cdot kg \cdot s^{-2}$
電界の強さ	ボルト毎メートル	V/m	$m \cdot kg \cdot s^{-3} \cdot A^{-1}$
体積電荷	クーロン毎立方メートル	C/m^3	$m^{-3} \cdot s \cdot A$
電気変位	クーロン毎平方メートル	C/m^2	$m^{-2} \cdot s \cdot A$
誘電率	ファラド毎メートル	F/m	$m^{-3} \cdot kg^{-1} \cdot s^4 \cdot A^2$
透磁率	ヘンリー毎メートル	H/m	$m \cdot kg \cdot s^{-2} \cdot A^{-2}$
モルエネルギー	ジュール毎モル	J/mol	$m^2 \cdot kg \cdot s^{-2} \cdot mol^{-1}$
モルエントロピー，モル熱容量	ジュール毎モル毎ケルビン	J/(mol・K)	$m^2 \cdot kg \cdot s^{-2} \cdot K^{-1} \cdot mol^{-1}$
照射線量（Ｘ線及びγ線）	クーロン毎キログラム	C/kg	$kg^{-1} \cdot s \cdot A$
吸収線量率	グレイ毎秒	Gy/s	$m^2 \cdot s^{-3}$
放射強度	ワット毎ステラジアン	W/sr	$m^4 \cdot m^{-2} \cdot kg \cdot s^{-3}=m^2 \cdot kg \cdot s^{-3}$
放射輝度	ワット毎平方メートル毎ステラジアン	$W/(m^2 \cdot sr)$	$m^2 \cdot m^{-2} \cdot kg \cdot s^{-3}=kg \cdot s^{-3}$

表６．国際単位系と併用されるが国際単位系に属さない単位

名称	記号	SI 単位による値
分	min	1 min=60s
時	h	1h =60 min=3600 s
日	d	1 d=24 h=86400 s
度	°	1° =(π/180) rad
分	’	1’ =(1/60)° =(π/10800) rad
秒	”	1” =(1/60)’ =(π/648000) rad
リットル	l、L	$1l=1\ dm^3=10^{-3}m^3$
トン	t	$1t=10^3\ kg$
ネーパ	Np	1Np=1
ベル	B	1B=(1/2)ln10(Np)

表７．国際単位系と併用されこれに属さない単位でSI単位で表される数値が実験的に得られるもの

名称	記号	SI 単位であらわされる数値
電子ボルト	eV	$1eV=1.60217733(49) \times 10^{-19}J$
統一原子質量単位	u	$1u=1.6605402(10) \times 10^{-27}kg$
天文単位	ua	$1ua=1.49597870691(30) \times 10^{11}m$

表８．国際単位系に属さないが国際単位系と併用されるその他の単位

名称	記号	SI 単位であらわされる数値
海里		１海里=1852m
ノット		１ノット=１海里毎時=(1852/3600)m/s
アール	a	$1\ a=1\ dam^2=10^2m^2$
ヘクタール	ha	$1\ ha=1\ hm^2=10^4m^2$
バール	bar	$1\ bar=0.1MPa=100kPa=1000hPa=10^5Pa$
オングストローム	Å	$1\ Å=0.1nm=10^{-10}m$
バーン	b	$1\ b=100fm^2=10^{-28}m^2$

表９．固有の名称を含むCGS組立単位

名称	記号	SI 単位であらわされる数値
エルグ	erg	$1\ erg=10^{-7}\ J$
ダイン	dyn	$1\ dyn=10^{-5}N$
ポアズ	P	$1\ P=1\ dyn \cdot s/cm^2=0.1Pa \cdot s$
ストークス	St	$1\ St\ =1cm^2/s=10^{-4}m^2/s$
ガウス	G	$1\ G\ \hat{}10^{-4}T$
エルステッド	Oe	$1\ Oe\ \hat{}(1000/4\pi)A/m$
マクスウェル	Mx	$1\ Mx\ \hat{}10^{-8}Wb$
スチルブ	sb	$1\ sb\ =1cd/cm^2=10^4cd/m^2$
ホト	ph	$1\ ph=10^4lx$
ガル	Gal	$1\ Gal\ =1cm/s^2=10^{-2}m/s^2$

表10．国際単位に属さないその他の単位の例

名称	記号	SI 単位であらわされる数値
キュリー	Ci	$1\ Ci=3.7 \times 10^{10}Bq$
レントゲン	R	$1\ R\ =\ 2.58 \times 10^{-4}C/kg$
ラド	rad	$1\ rad=1cGy=10^{-2}Gy$
レム	rem	$1\ rem=1\ cSv=10^{-2}Sv$
X線単位		$1X\ unit=1.002 \times 10^{-4}nm$
ガンマ	γ	$1\gamma=1\ nT=10^{-9}T$
ジャンスキー	Jy	$1\ Jy=10^{-26}W \cdot m^{-2} \cdot Hz^{-1}$
フェルミ		$1\ fermi=1\ fm=10^{-15}m$
メートル系カラット		$1\ metric\ carat\ =\ 200\ mg\ =\ 2 \times 10^{-4}kg$
トル	Torr	1 Torr = (101 325/760) Pa
標準大気圧	atm	1 atm = 101 325 Pa
カロリー	cal	
ミクロン	μ	$1\ \mu\ =1\mu m=10^{-6}m$

（第７版，1998年改訂）